

Domain-Shared Learning and Gradual Alignment for Unsupervised Domain Adaptation Visible-Infrared Person Re-Identification

Nianchang Huang^{a,b}, Yi Xu^{a,b}, Ruida Xi^{a,b}, Qiang Zhang^{*a,b}

^aState Key Laboratory of Electromechanical Integrated Manufacturing of High-Performance Electronic Equipments, Xidian University, Xi'an, Shaanxi 710071, China

^bCenter for Complex Systems, School of Mechano-Electronic Engineering, Xidian University, Xi'an, Shaanxi 710071, China

Abstract

Recently, Visible-Infrared person Re-Identification (VI-ReID) has achieved remarkable performance on public datasets. However, due to the discrepancies between public datasets and real-world data, most existing VI-ReID algorithms struggle in real-life applications. To address this, we take the initiative to investigate Unsupervised Domain Adaptation Visible-Infrared person Re-Identification (UDA-VI-ReID), aiming to transfer the knowledge learned from the public data to real-world data without compromising accuracy and requiring the annotation of new samples. Specifically, we first analyze two basic challenges in UDA-VI-ReID, *i.e.*, inter-domain modality discrepancies and intra-domain modality discrepancies. Then, we design a novel two-stage model, *i.e.*, Domain-Shared Learning and Gradual Alignment (DSLGA), to handle these discrepancies. In the first pre-training stage, DSLGA introduces a Domain-Shared Learning Strategy (DSLS) to mitigate ineffective pre-training caused by inter-domain modality discrepancies via exploiting shared information between the source and target domains. While, in the second fine-tuning stage, DSLGA designs a Gradual Alignment Strategy (GAS) to handle the cross-modality alignment challenges between visible and infrared data caused by the large intra-domain modality discrepancies through a cluster-to-holistic alignment way. Finally, a new UDA-VI-ReID testing method *i.e.*, CMDA-XD, is constructed for training and testing different UDA-VI-ReID models. A large amount of experiments demonstrate that our method significantly outperforms existing domain adaptation methods for VI-ReID and even some supervised methods under various settings.

Keywords: Visible-infrared person re-identification, Unsupervised domain adaptation, Domain-shared exploration, Cluster-to-holistic alignment

*Corresponding author: Qiang Zhang.

Email addresses: huangnianchang@xidian.edu.cn (Nianchang Huang), yi_xu@stu.xidian.edu.cn (Yi Xu), ruidaxi@stu.xidian.edu.cn (Ruida Xi), qzhang@xidian.edu.cn (Qiang Zhang*)

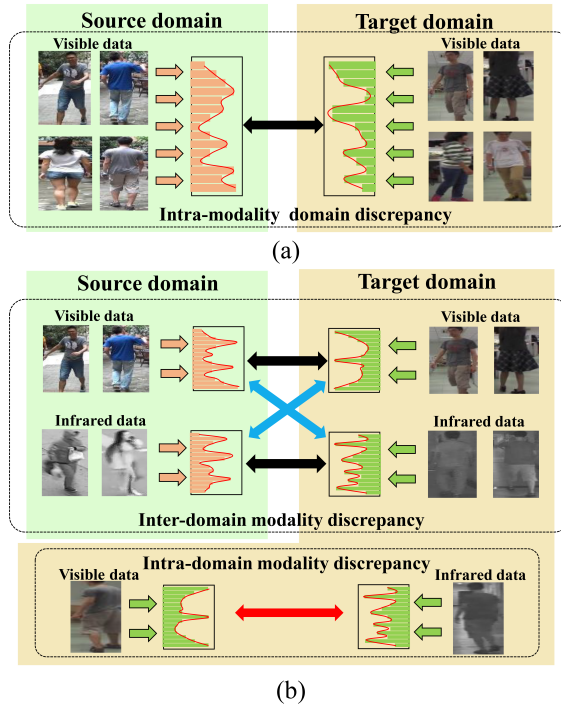


Fig. 1: Comparisons between UDA-ReID and UDA-VI-ReID. (a) The intra-modality domain discrepancies in UDA-ReID. (b) The inter-domain modality discrepancies and intra-domain modality discrepancies in UDA-VI-ReID. Arrows in different colors mean different types of discrepancies

1. Introduction

Recently, VI-ReID algorithms have obtained significant improvements, which have surpassed humans by a large margin on some public datasets [1, 2]. However, directly applying those VI-ReID algorithms to real-life applications usually results in a significant decline in accuracy because of the huge distribution discrepancies between training data from publicly available datasets and real-world ones. A straightforward way to address such an issue is to label images in real-life applications and re-train those VI-ReID algorithms. However, the cost of annotating a large dataset is usually very high. Naturally, a question is raised: *can we develop strategies to transfer the knowledge learned from public data to real-world data without compromising accuracy and requiring new annotations?* Unsupervised Domain Adaptation ReID (UDA-ReID) is such a task that aims to transfer the learned knowledge from the source domain to the target domain. However, existing UDA-ReID methods[3, 4] mainly focuses on single-modality data, *i.e.*, UDA-VV-ReID. Unsupervised Domain Adaptation VI-ReID (UDA-VI-ReID) models are rarely investigated in existing research. Considering that, we take the initiative to investigate UDA-VI-ReID in this paper.

As shown in Fig. 1 (b), the inter-domain modality discrepancies are the major challenge in UDA-VI-ReID, which refers to that UDA-VI-ReID simultaneously encounters

intra-modality and inter-modality domain discrepancies across the source and target domains (*i.e.*, the black and blue arrows, respectively, in Fig. 1(b)), rather than just intra-modality domain discrepancies as in single-modality UDA-ReID (*i.e.*, the black arrow in Fig. 1 (a)). Meanwhile, the intra-domain modality discrepancies refer to the fact that even within the same domain in UDA-VI-ReID, the modality discrepancies will also hinder the learning of those discriminative person features (*i.e.*, the red arrow in Fig. 1 (b)), especially when the ground-truth labels of the target domain data are absent during training.

The inter- and intra-domain modality discrepancies will make existing single-modality UDA-ReID methods [5, 3, 4] suffer in UDA-VI-ReID if without any modifications. To address these challenges, this paper proposes a preliminary solution for UDA-VI-ReID based on the classic clustering-based UDA-ReID framework, which usually first pre-trains a ReID network on the source domain data via some supervised learning strategies, and then fine-tunes the pre-trained network on the target domain data, following a clustering-based pseudo label generation and pseudo label-based network optimization iterative paradigm.

However, such a framework faces the following issues when directly applied to the UDA-VI-ReID task. First, the VI-ReID network pre-trained on the source domain data may suffer a decline in feature extraction capability when used on target domain data due to inter-domain modality discrepancies. Especially, the feature extraction ability of a VI-ReID network pre-trained on the source domain data may be only slightly better than that of a randomly initialized VI-ReID network, when directly applied to the target domain data. Secondly, the core of the fine-tuning stage is to generate high-quality pseudo labels for unlabeled target domain data and use them to optimize the performance of the pre-trained network. While generating pseudo labels within the same modality is relatively straightforward, aligning labels of the same identity across modalities (*i.e.*, addressing the cross-modality alignment challenges) is much more difficult due to significant intra-domain modality discrepancies. Those incorrectly matched visible-infrared clusters will easily lead to training bias and sub-optimal results. To address the aforementioned issues, this paper proposes a novel two-stage UDA-VI-ReID method, namely the Domain Shared Learning and Gradual Alignment (DSLGA).

In the pre-training stage, DSLGA realizes that, beyond their own specific information, the source and target domains inherently share some common information (*e.g.*, person shapes and contours), and accordingly designs a Domain-Shared Learning Strategy (DLS) to leverage such domain-shared information for reducing their inter-domain modality discrepancies. Specifically, DLS first projects the features extracted from the two domains, respectively, into the same feature space to capture their domain-shared information by using a parameter-shared VI-ReID network. Then, DLS specially designs a Domain-Shared Adversarial Loss (DSAL) to pull close the distributions of the source and target domains in a united feature space via a generative adversarial way, thus facilitating the extraction of domain-shared information. Moreover, DSLGA incorporates a Cluster Refinement with Multiple Results (CRM) module, which is specifically designed to generate more reliable intra-modality pseudo labels for each modality within the target domain.

In the fine-tuning stage, DSLGA introduces a Gradual Alignment Strategy (GAS)

to gradually overcome intra-domain modality discrepancies, spanning from cluster-level alignment for cross-modality pseudo label generation to holistic-level alignment for VI-ReID network optimization. Specifically, GAS first presents a Supplementary Graph Matching (SGM) module to tackle cross-modality alignment challenges and generate high-quality cross-modality pseudo labels for target domain data. Especially, beyond the classic paradigm inter-modality alignment, SGM innovatively proposes an intra-modality supplementary alignment step for those cross-modality unaligned clusters, aiming to realign them with their closest intra-modality clusters. This further exploits such unaligned clusters, especially for those being over-clustered ones. Then, when training the VI-ReID network, GAS further designs a Cross-Modality Consistency Constraining (CMCC) module to suppress those incorrect pseudo labels that are inevitably produced by SGM. The core of CMCC lies in utilizing all person information within the source and target domains (*i.e.*, holistic information) to assess the confidence levels of the generated pseudo labels, subsequently suppressing those pseudo labels with lower confidence and reinforcing those with higher confidence.

Furthermore, we also construct a new CMDA-XD testing method on top of some existing cross-modality datasets for UDA-VI-ReID in this paper. Overall, the contributions of this paper can be summarized as follows:

- This paper takes the initiative to investigate the unsupervised domain adaptation VI-ReID, aiming to transfer the knowledge learned from the source domain data to the target domain data without requiring the annotation of new samples. Accordingly, a novel UDA-VI-ReID model DSLGA is proposed and a new testing method CMDA-XD is constructed in this paper.
- We design a DSLS in the pre-training stage to alleviate the inter-domain modality discrepancies and obtain a well-initialized network for the target domain by exploring the domain-shared information between the source and target domains.
- We present a GAS to overcome the large intra-domain modality discrepancies through a cluster-to-holistic alignment way, thus significantly boosting the performance of our model on target domain data.

2. Related Work

2.1. Supervised Visible-Infrate Person Re-Identification

Most existing VI-ReID models can be divided into two categories: modality-specific information compensation based models [6] and modality-shared feature learning based models [7, 8]. Specifically, modality-specific information compensation based models follow a two-stage strategy. They first handle cross-modality discrepancies by generating information for the missing modalities from the existing ones, thus enabling them to achieve (RGB-T)-to-(RGB-T) matching. Then, they capture discriminative cross-modality complementary information from paired RGB-T images to address intra-modality variations. For example, Zhang *et al.* [6] proposed feature-level modality-specific information generation rather than image-level generation for VI-ReID. For that, they first decompose the single-modality RGB (IR) features into modality-specific

RGB (IR) features and modality-shared RGB (IR) features. Then, they generate the missing modality-specific IR (RGB) features from those decomposed modality-shared RGB (IR) features by presenting a Feature-level Modality Compensation (FMC) module. Eventually, they combine three types of features for matching.

Differently, modality-shared feature learning based models try to simultaneously address the intra-modality variations and inter-modality variations by capturing those discriminative person-related features co-existing in the two modalities. For example, Liu *et al.* [9] developed a shareable dual-path information-preserving network to extract 3D-shaped middle-level shareable feature vectors, aiding the model in learning discriminative feature representations.

However, the current VI-ReID algorithms are tailored to specific datasets. When these algorithms are applied to real-world applications, their accuracies will experience a notable decline due to the substantial distribution variations between public data and real-world data. In this paper, we will introduce a pioneering UDA-VI-ReID task to address this issue.

2.2. Unsupervised Domain Adaptation Person Re-Identification

Generally speaking, existing UDA-ReID models can be divided into two categories: domain transformation-based models [5] and pseudo label-based models [3, 4]. Domain transformation-based models are based on the idea of image style transformation, which tries to reduce domain discrepancies by migrating the image styles from the source domain to the target domain. During this process, their learned knowledge in the source domain will be also transferred to the target domain, thus being able to rightly identify different persons for the target domain data. For example, Huang *et al.* [10] used a Suppression of Background Shift Generative Adversarial Network (SBS-GAN) to generate images with the background being suppressed, thus mitigating the data gaps between the source and target domains. They further proposed a Densely Associated 2-Stream (DA-2S) network with an update strategy to learn discriminative ID features from the generated data, which considers both the human-body information and certain useful ID-related cues in the background.

On the other hand, pseudo label-based models [4] first pre-train a model with source domain data via supervised methods, and then iterate them between clustering and fine-tuning on the target domain data. For instance, Chen *et al.* [11] designed a Mutual Mean-Teaching (MMT) based on a pseudo label generation strategy, which uses clustering algorithms to assign labels to every sample and the teacher-student model to suppress data noise. He *et al.* [12] focused on the pseudo label generation strategy during the fine-tuning stage, since the qualities of those generated pseudo labels determine fine-tuning results. They argued that the consistency among different feature spaces is the key to the pseudo label’s qualities. Accordingly, a Self-Consistent pseudo label Refinement method (SECRET) was proposed to improve the consistency by mutually refining the pseudo labels generated from different feature spaces, resulting in more accurate pseudo labels.

Although existing UDA-ReID models have achieved great progress, those models will not work when facing the large inter- and intra-domain modality discrepancies within UDA-VI-ReID. Considering that, this paper takes the initiative to investigate

Unsupervised Domain Adaption Visible-Infrared person Re-Identification (UDA-VI-ReID).

2.3. Unsupervised Domain Adaptation Visible-Infrared Person Re-Identification

Recently, some other researchers also studied UDA-VI-ReID. Specifically, Yang *et al.* [13] proposed a Translation, Association and Augmentation (TAA) framework to transfer learned knowledge from the labeled visible source domain to the unlabelled visible-infrared target domain. For that, they first employed a modality translator to transfer visible images into infrared images, formulating generated visible-infrared image pairs for cross-modality supervised training. Then, a Robust Association and Mutual Learning (RAML) module and a Translation Supervision and Feature Augmentation (TSFA) module were designed to resist label noise and enhance feature discriminability, respectively.

Different from TAA that transfers the learned knowledge from the labeled visible source domain to the unlabeled visible-infrared target domain, this paper focuses on transferring the learned knowledge from the labeled visible-infrared source domain to the unlabeled visible-infrared target domain.

3. Methodology

The overall framework of our proposed Domain-Shared Learning and Gradual Alignment (DSLGA) is shown in Fig. 2, which mainly contains two stages: pre-training and fine-tuning. In the pre-training stage, a Domain-Shared Learning Strategy (DSLS) is designed to explore the domain-shared information across the source and target domains to address the inter-domain modality discrepancies. Especially, DSLS will design a Domain-Shared Adversarial Loss (DSAL) to pull close the distributions of the source and target domains in a united feature space via a generative adversarial way. Besides, a Cluster Refinement with Multiple Results (CRMR) module will be specifically designed to generate pseudo labels for addressing the label deficiency problem in the target domain. In the fine-tuning stage, a Gradual Alignment Strategy (GAS) will be presented to achieve cross-modality alignment, overcoming the intra-domain modality discrepancies within the target domain data. Especially, a Supplementary Graph Matching (SGM) module and a Cross-Modality Consistency Constraining (CMCC) module will be proposed in GAS to achieve cluster-level and holistic-level alignments, respectively. In the following contents, we will demonstrate the details of each module in our proposed method.

In this paper, we denote the source domain data by $D_s = \{D_{s,V}, D_{s,I}\}$ and the target domain data by $D_t = \{D_{t,V}, D_{t,I}\}$, respectively. Here,

$$D_{s,V} = \{(x_{s,V}^n, y_{s,V}^n) \mid n = 1, 2, \dots, N_{s,V}\} \quad (1)$$

represents the n -th visible image $x_{s,V}^n$ and its corresponding person identity $y_{s,V}^n$. $D_{s,I} = \{(x_{s,I}^n, y_{s,I}^n) \mid n = 1, 2, \dots, N_{s,I}\}$ represents the n -th infrared image $x_{s,I}^n$ and its corresponding person identity $y_{s,I}^n$. $N_{s,V}$ and $N_{s,I}$ denote the numbers of visible and infrared images within the source domain data, respectively. Moreover, we suppose that there

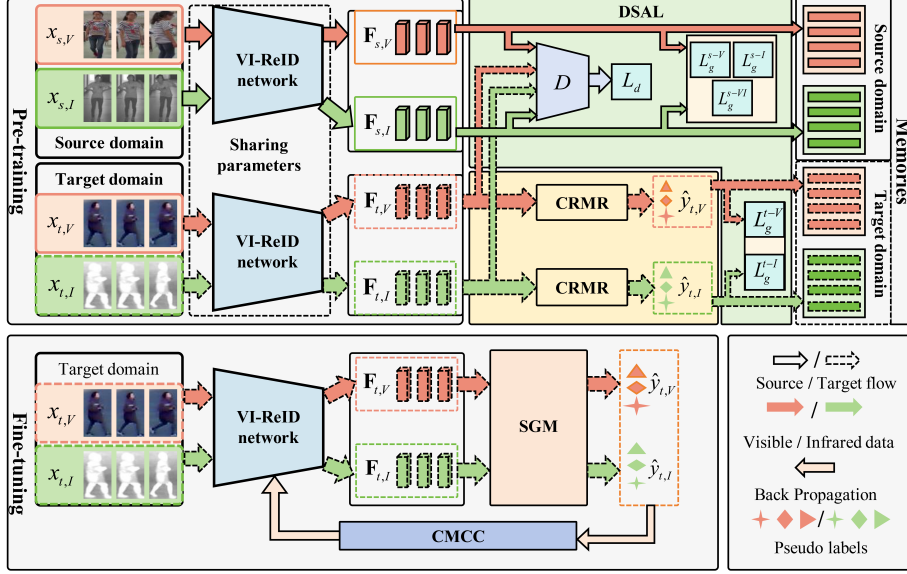


Fig. 2: Framework of our proposed DSLGA model. It contains two main stages, *i.e.*, pre-training and fine-tuning. In the pre-training stage, a VI-ReID network is trained to achieve the knowledge transfer from the source domain to the target domain. Especially, a domain-shared learning strategy (DSLS) is designed to mitigate the inter-domain modality discrepancies with the aid of the proposed DSAL. As well, a CRMR is proposed to generate intra-modality pseudo labels for the target domain. In the fine-tuning stage, the pre-trained model in the first state is further optimized by deeply exploring the target domain data. Especially, a gradual alignment strategy (GAS) is designed to mitigate the intra-domain modality discrepancies, which first generates cross-modality pseudo labels at the cluster level by an SGM module and then suppresses those incorrect pseudo labels at the holistic level by a CMCC module.

are C_s identities within the source domain data. Accordingly, $y_{s,V}^n$ and $y_{s,I}^n \in [1, C_s]$. Similarly, $D_{t,V} = \{x_{t,V}^n | n = 1, 2, \dots, N_{t,V}\}$ and $D_{t,I} = \{x_{t,I}^n | n = 1, 2, \dots, N_{t,I}\}$ represent the visible images and the infrared images in the target domain, respectively. It should be noted that the identity labels $y_{t,V}$ and $y_{t,I}$ for the visible and infrared images of the target domain data are missed. Therefore, in different training stages, we will generate their pseudo labels $\hat{y}_{t,V}$ and $\hat{y}_{t,I}$ via some algorithms to replace $y_{t,V}$ and $y_{t,I}$, respectively. The numbers of identities within the pseudo labels $\hat{y}_{t,V}$ and $\hat{y}_{t,I}$ are denoted by $C_{t,V}$ and $C_{t,I}$, respectively. Subsequently, for a better introduction in the following content, we denote the target domain data with its corresponding pseudo labels by $\hat{D}_t = \{\hat{D}_{t,V}, \hat{D}_{t,I}\}$, where $\hat{D}_{t,V} = \{(x_{t,V}^n, \hat{y}_{t,V}^n) | n = 1, 2, \dots, N_{t,V}\}$ and $\hat{D}_{t,I} = \{(x_{t,I}^n, \hat{y}_{t,I}^n) | n = 1, 2, \dots, N_{t,I}\}$. Here $\hat{y}_{t,V}^n \in [1, C_{t,V}]$ and $\hat{y}_{t,I}^n \in [1, C_{t,I}]$.

3.1. VI-ReID Network

As shown in Fig. 3 (a), our VI-ReID network follows the classical specific-shared feature extraction structure, which is similar to most existing VI-ReID models[1, 14]. Specifically, it first employs two modality-specific feature extraction subnetworks to extract visible features \hat{F}_V and infrared features \hat{F}_I from visible images and infrared

images, respectively, *i.e.*,

$$\hat{\mathbf{F}}_V = f_{V,sp}(x_V, \phi_{V,sp}), \hat{\mathbf{F}}_I = f_{I,sp}(x_I, \phi_{I,sp}), \quad (2)$$

where $f_{V,sp}(*, \phi_{V,sp})$ and $f_{I,sp}(*, \phi_{I,sp})$ denote two modality-specific feature extraction subnetworks with their parameters $\phi_{V,sp}$ and $\phi_{I,sp}$, respectively. x_V and x_I denote all visible images and infrared images, respectively, from either the source or target domain data. Then, the extracted modality-specific features $\hat{\mathbf{F}}_V$ or $\hat{\mathbf{F}}_I$ are fed into a modality-shared feature extraction subnetwork to obtain their person features $\mathbf{F}_V \in \mathbb{R}^{N_{s,V} \times D}$ ($\mathbf{F}_V \in \mathbb{R}^{N_{t,V} \times D}$) or $\mathbf{F}_I \in \mathbb{R}^{N_{s,I} \times D}$ ($\mathbf{F}_I \in \mathbb{R}^{N_{t,I} \times D}$) in a modality-shared feature space, *i.e.*,

$$\mathbf{F}_V = f_{sh}(\hat{\mathbf{F}}_V, \phi_{sh}), \mathbf{F}_I = f_{sh}(\hat{\mathbf{F}}_I, \phi_{sh}). \quad (3)$$

Here, $f_{sh}(*, \phi_{sh})$ denotes the modality-shared subnetwork with its parameters ϕ_{sh} , which remains unchanged across different modalities. D denotes the channels. For simplicity, we denote the VI-ReID network by $f_\phi(*, \phi)$ with $\phi = \{\phi_{V,sp}, \phi_{I,sp}, \phi_{sh}\}$.

Besides the VI-ReID network, two memory modules are employed for the source domain data, and another two memory modules are employed for the target domain data to store the visible and infrared feature centers of each identity, respectively. These stored feature centers will be employed to assist in different training stages in the subsequent sections. Considering that the four memory modules follow the same structure, we take the memory module constructed for the visible samples in the source domain as an example for introduction in the following contents.

Specially, given the visible images in the source domain $D_{s,V}$, the memory module includes a center memory $\mathbb{M}_{s,V} \in \mathbb{R}^{C_s \times D}$ along with an initialization operation and an update operation. Here, each item $\mathbb{M}_{s,V}[c_s] \in \mathbb{R}^{1 \times D}$ in $\mathbb{M}_{s,V}$ denotes the visible feature center of the c_s -th identity in the source domain data. In different training steps or stages, the center memory $\mathbb{M}_{s,V}$ is initialized or updated by the following steps.

First, the visible features $\mathbf{F}_{s,V}^{c_s, n_{c_s}} \in \mathbb{R}^{1 \times D}$ for the n_{c_s} -th visible image of the c_s -th identity are extracted by

$$\mathbf{F}_{s,V}^{c_s, n_{c_s}} = f_\phi(x_{s,V}^{c_s, n_{c_s}}, \phi), \quad (4)$$

where $n_{c_s} \in [1, N_{s,V}^{c_s}]$ and $N_{s,V}^{c_s}$ denotes the total number of visible images of the c_s -th identity. Then, the feature center $\mathbf{F}_{s,V,center}^{c_s}$ of the c_s -th identity is computed by

$$\mathbf{F}_{s,V,center}^{c_s} = \frac{1}{N_{s,V}^{c_s}} \sum_{n_{c_s}=1}^{N_{s,V}^{c_s}} \mathbf{F}_{s,V}^{c_s, n_{c_s}}. \quad (5)$$

For the initialization operation, the center memory $\mathbb{M}_{s,V}[c_s]$ is initialized by

$$\mathbb{M}_{s,V}[c_s] = \mathbf{F}_{s,V,center}^{c_s}. \quad (6)$$

While, for the update operation, the center memory $\mathbb{M}_{s,V}[c_s]$ is updated by

$$\mathbb{M}_{s,V}[c_s] = \alpha \mathbb{M}_{s,V}[c_s] + (1 - \alpha) \mathbf{F}_{s,V,center}^{c_s}, \quad (7)$$

where α denotes the update rate and is set to 0.5 in this paper.

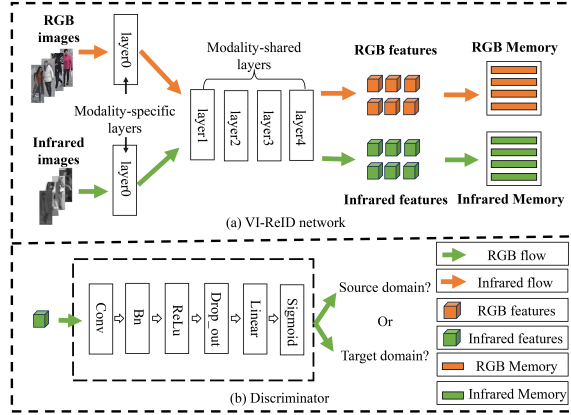


Fig. 3: Structures of the VI-ReID network and the discriminator. (a) The VI-ReID network. (b) The discriminator. Items in different colors represent different person identities.

Similarly, we can obtain the infrared feature center memory with C_s items $\mathbb{M}_{s,I} \in \mathbb{R}^{C_s \times D}$ for the source domain data, the visible feature center memory with $C_{t,V}$ items $\mathbb{M}_{t,V} \in \mathbb{R}^{C_{t,V} \times D}$ and the infrared feature center memory with $C_{t,I}$ items $\mathbb{M}_{t,I} \in \mathbb{R}^{C_{t,I} \times D}$ for the target domain data, respectively.

3.2. Domain-Shared Learning Strategy in Pre-training stage

The significant inter-domain modality differences between data across the source and target domains usually result in a fact that the VI-ReID network, pre-trained on the source domain data, usually obtains undesirable results when directly applied to the target domain data. Considering that, a novel Domain-Shared Learning Strategy (DSLS) is designed in this subsection to address such an issue by exploring domain-shared information between the source and target domains.

Specifically, DSLS aims at exploring the domain-shared information to bridge the source and target domains in the pre-training stage. For that, DSLS first introduces target domain data \hat{D}_t along with source domain data D_s for assisting the pre-training of the VI-ReID network. Then, DSLS extracts the features from source domain data D_s and target domain data \hat{D}_t through two identical VI-ReID networks $f_\phi(*, \phi)$, *i.e.*,

$$\begin{aligned} \mathbf{F}_{s,V} &= f_\phi(x_{s,V}, \phi), \mathbf{F}_{s,I} = f_\phi(x_{s,I}, \phi), \\ \mathbf{F}_{t,V} &= f_\phi(x_{t,V}, \phi), \mathbf{F}_{t,I} = f_\phi(x_{t,I}, \phi), \end{aligned} \quad (8)$$

where $\mathbf{F}_{s,V} \in \mathbb{R}^{N_{s,V} \times D}$, $\mathbf{F}_{s,I} \in \mathbb{R}^{N_{s,I} \times D}$, $\mathbf{F}_{t,V} \in \mathbb{R}^{N_{t,V} \times D}$ and $\mathbf{F}_{t,I} \in \mathbb{R}^{N_{t,I} \times D}$ denote the person features of visible images and infrared images within the source and target domains, respectively.

After that, a novel Domain-Shared Adversarial Loss (DSAL) will be specially designed to constrain the identity distances across the two domains in an adversarial learning way [15], which can diminish the disparities between the features from the source domain and those from the target domain. As well, DSAL will also preserve the

distinctions among different person identities in both the source and target domains for facilitating the extraction of domain-shared information, *i.e.*,

$$\mathcal{L}_{DSAL} = \text{DSAL}(\mathbf{F}_{s,V}, \mathbf{F}_{s,I}, \mathbf{F}_{t,V}, \mathbf{F}_{t,I}, y_{s,V}, y_{s,I}, y_{t,V}, y_{t,I}). \quad (9)$$

It should be noted that the labels $y_{t,V}$ and $y_{t,I}$ for target domain data are absent. Therefore, a Cluster Refinement with Multiple Results (CRMR) module will be further designed to generate their pseudo labels $\hat{y}_{t,V}$ and $\hat{y}_{t,I}$ for target domain data to replace $y_{t,V}$ and $y_{t,I}$ before each training epoch, which will be described in detail subsequently.

3.2.1. Domain-Shared Adversarial Loss (DSAL)

For adversarial learning, DSAL first treats the VI-ReID network $f_\phi(*, \phi)$ as the generator, and then designs a classifier $\text{Class}(*, \varrho)$ with its parameters ϱ as the discriminator. As shown in Figure 3 (b), the discriminator takes the features extracted from the input images by the VI-ReID network as inputs and outputs the probability of the inputs belonging to the target domain. During the training processes of discriminator $\text{Class}(*, \varrho)$, we fix the parameters of the generator $f_\phi(*, \phi)$ and optimize the discriminator $\text{Class}(*, \varrho)$ by using the cross-entropy loss, *i.e.*,

$$L_d = -\frac{1}{N_{all}} \sum_{n=1}^{N_{all}} (dom_n \log(\text{Class}(f_\phi(x^n, \phi), \varrho)) + (1 - dom_n) \log(1 - \text{Class}(f_\phi(x^n, \phi), \varrho))), \quad (10)$$

where dom_n denotes the domain label of the sample x^n . $N_{all} = N_{s,V} + N_{s,I} + N_{t,V} + N_{t,I}$ is the total number of samples in the source and target domains. When training the generator $f_\phi(*, \phi)$, we fix the parameters of discriminators $\text{Class}(*, \varrho)$ and optimize the generator $f_\phi(*, \phi)$ to prevent the discriminator from distinguishing the right domains, *i.e.*,

$$L_g = \frac{1}{N_{all}} \sum_{n=1}^{N_{all}} (\text{Class}(f_\phi(x^n, \phi), \varrho) - 0.5)^2. \quad (11)$$

Besides, some contrastive losses are also performed on the generator to preserve the distinctions among different person identities. Different from conventional contrastive losses that separately constrain features in the source and target domains, our DSAL **constraints all visible and infrared feature distances within a unified feature space**, thereby explicitly promoting the extraction of domain-invariant features. Specifically, DSAL first concatenates the visible (infrared) feature center memories $\mathbb{M}_{s,V}$ and $\mathbb{M}_{t,V}$ (or $\mathbb{M}_{s,I}$ and $\mathbb{M}_{t,I}$) from the source domain data and target domain data, obtaining:

$$\begin{aligned} \mathbb{M}_{st,V} &= \text{Cat}(\mathbb{M}_{s,V}, \mathbb{M}_{t,V}), \\ \mathbb{M}_{st,I} &= \text{Cat}(\mathbb{M}_{s,I}, \mathbb{M}_{t,I}), \end{aligned} \quad (12)$$

where $\mathbb{M}_{st,V}$ and $\mathbb{M}_{st,I}$ denote the concatenated visible and infrared feature center memories, respectively. $\text{Cat}(*)$ denotes the concatenation operation.

Then, DSAL introduces the intra-modality constraints on the visible features of the source domain data in the domain-shared feature space $\mathbb{M}_{st,V}$, *i.e.*,

$$\mathcal{L}_g^{s-V} = -\log \sum_{n=1}^{N_{s,V}} \frac{e^{(\mathbf{F}_{s,V}^n \mathbb{M}_{st,V}^T [y_{s,V}^n])}}{\sum_{k=1}^{C_s+C_{t,V}} e^{(\mathbf{F}_{s,V}^n \mathbb{M}_{st,V}^T [k])}}, \quad (13)$$

where $\mathbf{F}_{s,V}^n$ represents the features of the n -th visible image $x_{s,V}^n$ in the source domain, $(*)^T$ means the transpose operation. Similarly, a constraint \mathcal{L}_g^{s-I} is also performed on the infrared features within the source domain data in the domain-shared space $\mathbb{M}_{st,I}$, *i.e.*,

$$\mathcal{L}_g^{s-I} = -\log \sum_{n=1}^{N_{s,I}} \frac{e^{(\mathbf{F}_{s,I}^n \mathbb{M}_{st,I}^T [y_{s,I}^n])}}{\sum_{k=1}^{C_s+C_{t,I}} e^{(\mathbf{F}_{s,I}^n \mathbb{M}_{st,I}^T [k])}}. \quad (14)$$

After that, DSAL also builds the inter-modality constraints for the source domain data in the domain-shared feature space to better utilize information in the source domain *i.e.*,

$$\mathcal{L}_g^{s-VI} = -\log \sum_{n=1}^{N_{s,V}} \frac{e^{(\mathbf{F}_{s,V}^n \mathbb{M}_{st,I}^T [y_{s,V}^n])}}{\sum_{k=1}^{C_s+C_{t,I}} e^{(\mathbf{F}_{s,V}^n \mathbb{M}_{st,I}^T [k])}} - \log \sum_{n=1}^{N_{s,I}} \frac{e^{(\mathbf{F}_{s,I}^n \mathbb{M}_{st,V}^T [y_{s,I}^n])}}{\sum_{k=1}^{C_s+C_{t,V}} e^{(\mathbf{F}_{s,I}^n \mathbb{M}_{st,V}^T [k])}}. \quad (15)$$

What's more, DSAL also performs some intra-modality constraints on the target domain data, *i.e.*,

$$\mathcal{L}_g^{t-V} = -\log \sum_{n=1}^{N_{t,V}} \frac{e^{(\mathbf{F}_{t,V}^n \mathbb{M}_{st,V}^T [y_{t,V}^n])}}{\sum_{k=1}^{C_s+C_{t,V}} e^{(\mathbf{F}_{t,V}^n \mathbb{M}_{st,V}^T [k])}}, \quad (16)$$

$$\mathcal{L}_g^{t-I} = -\log \sum_{n=1}^{N_{t,I}} \frac{e^{(\mathbf{F}_{t,I}^n \mathbb{M}_{st,I}^T [y_{t,I}^n])}}{\sum_{k=1}^{C_s+C_{t,I}} e^{(\mathbf{F}_{t,I}^n \mathbb{M}_{st,I}^T [k])}}. \quad (17)$$

It is important to note that in this stage, the absence of ground truth in the target domain will result in significant noise among the visible and infrared modalities. Consequently, we have refrained from introducing inter-modality constraints in the target domain.

Accordingly, DSAL is expressed by

$$\mathcal{L}_{DSAL} = \mathcal{L}_d + \mathcal{L}_g + \mathcal{L}_g^{s-V} + \mathcal{L}_g^{s-I} + \mathcal{L}_g^{s-VI} + \mathcal{L}_g^{t-V} + \mathcal{L}_g^{t-I}. \quad (18)$$

In summary, by employing L_g and L_d with Eq. (10) and Eq.(11), DSAL pulls close the source and target domains in an adversarial learning way. Meanwhile, via the unified feature space designed in Eq. (12), DSAL can constrain all pedestrian embeddings in a shared feature space, which further effectively mitigates inter-domain modality discrepancies in the UDA-VI-ReID.

3.2.2. Cluster Refinement with Multiple Results (CRMR)

As shown in Fig. 4, CRMR aims at generating pseudo labels for visible and infrared data, respectively, in the target domain to assist the pre-training of the VI-ReID network. Specifically, we find that DBSCAN[16], a widely-used clustering algorithm for pseudo labels generation in unsupervised ReID[11, 12], is very sensitive to the

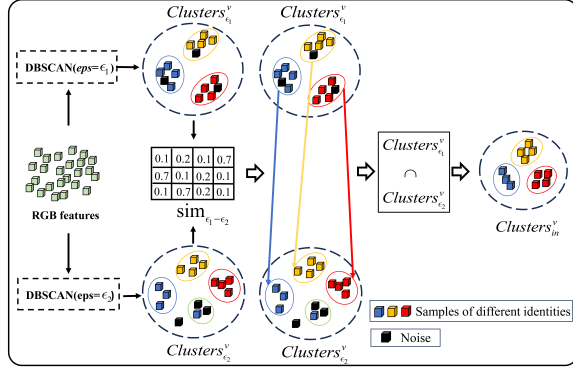


Fig. 4: Illustration of the proposed CRMR module. Samples in different colors represent different person identities.

hyperparameter neighborhood radius esp , *i.e.*, the maximum distance for one sample to be considered as in the neighborhood of the other sample. Generally speaking, a smaller esp can achieve better intra-cluster consistency, but it is easier to separate the samples of the same identity into different clusters. A larger esp usually results in fewer cluster centers and may cluster the samples of different identities into the same identity. Moreover, the clusters obtained from a small esp and those from a large esp are complementary to each other to some extent. Based on that, our proposed CRMR will explore the mutual relations among multiple clustering results obtained by using different esp settings to yield more reliable pseudo labels. Considering the way of generating pseudo labels for visible data is similar to that for infrared data, we take the visible data as an example for better explanation in the following sections.

Specifically, given the visible images in the target domain $D_{t,V}$, our proposed CRMR first extracts their features $\mathbf{F}_{t,V} \in \mathbb{R}^{N_{t,V} \times D}$ by

$$\mathbf{F}_{t,V} = f_{\phi}(x_{t,V}, \phi). \quad (19)$$

Then, two sets of clustering results ($Clusters_{\epsilon_1}$ and $Clusters_{\epsilon_2}$) will be obtained by feeding the visible features $\mathbf{F}_{t,V}$ into the DBSCAN algorithm with two different esp values, *i.e.*, ϵ_1 and ϵ_2 (suppose that $\epsilon_1 > \epsilon_2$), respectively, *i.e.*,

$$\begin{aligned} Clusters_{\epsilon_1}^v &= DBSCAN(\mathbf{F}_{t,V}, \epsilon_1), \\ Clusters_{\epsilon_2}^v &= DBSCAN(\mathbf{F}_{t,V}, \epsilon_2). \end{aligned} \quad (20)$$

Here, $Clusters_{\epsilon_1}^v$ and $Clusters_{\epsilon_2}^v$ contain K_{ϵ_1} and K_{ϵ_2} clusters, respectively and $K_{\epsilon_1} \leq K_{\epsilon_2}$. After that, for each cluster (*e.g.*, the k -th cluster) $cluster_{\epsilon_1,k}^v$ within $Clusters_{\epsilon_1}^v$, its centroid $u_{\epsilon_1,k}^v \in \mathbb{R}^{1 \times D}$ can be calculated by

$$u_{\epsilon_1,k}^v = \frac{1}{\mathcal{N}(cluster_{\epsilon_1,k}^v)} \sum_{\mathbf{F}_{t,V}^n \in cluster_{\epsilon_1,k}^v} \mathbf{F}_{t,V}^n, \quad (21)$$

where $\mathcal{N}(\ast)$ denotes the function that returns the number of the items within the input cluster. Accordingly, the centroids $u_{\epsilon_1}^v \in \mathbb{R}^{K_{\epsilon_1} \times D}$ of all clusters can be obtained by

$$u_{\epsilon_1}^v = \text{Cat}(u_{\epsilon_1,1}^v, u_{\epsilon_1,2}^v, \dots, u_{\epsilon_1, K_{\epsilon_1}}^v). \quad (22)$$

Furthermore, the centroids $u_{\epsilon_2}^v \in \mathbb{R}^{K_{\epsilon_2} \times D}$ of all clusters within the clusters $Clusters_{\epsilon_2}$ can also be computed in the same way.

Next, CRMR finds the nearest centroid pairs across the two clusters $Clusters_{\epsilon_1}$ and $Clusters_{\epsilon_2}$. For the k -th centroid in $Clusters_{\epsilon_1}$, *i.e.*, $u_{\epsilon_1,k}^v$, its similarities with the q -th centroid in $Clusters_{\epsilon_2}$, *i.e.*, $u_{\epsilon_2,q}^v$, will be computed by

$$\text{sim}_{\epsilon_1-\epsilon_2}(k, q) = \frac{u_{\epsilon_1,k}^v u_{\epsilon_2,q}^{vT}}{|u_{\epsilon_1,k}^v| \times |u_{\epsilon_2,q}^v|}, \quad (23)$$

where $| \ast |$ denotes the magnitude of a vector and \times means numerical multiplication. A higher similarity between two centroids means that the two centroids belong to the same person identity more probably. Based on that, the nearest centroid index q^* for $u_{\epsilon_1,k}^v$ will be obtained by

$$q^* = \underset{q}{\text{argmax}} \text{sim}_{\epsilon_1-\epsilon_2}(k, q). \quad (24)$$

Following that, the intersection set $cluster_{in,k}^v$ of $cluster_{\epsilon_1,k}^v$ and $cluster_{\epsilon_2,q^*}^v$ is considered as the reliable samples and will be saved, *i.e.*,

$$cluster_{in,k}^v = cluster_{\epsilon_1,k}^v \cap cluster_{\epsilon_2,q^*}^v. \quad (25)$$

Finally, we can obtain more reliable clustering results within visible data in the target domain, *i.e.*, $Clusters_{in}^v = \{cluster_{in,k}^v \mid k = 1, 2, \dots, K_{\epsilon_1}\}$ and assign the same pseudo labels to those samples in $cluster_{in,k}^v$.

3.3. Gradual Alignment Strategy in Fine-tuning stage

After obtaining the well-initialized VI-ReID network by using the proposed DSLS, the next step is to fine-tune the VI-ReID network in the target domain to improve its performance. The core of this step is how to find the potential corresponding cross-modality clusters and assign them with the same identity. However, the large intra-domain modality discrepancies across those unlabeled visible and infrared images will easily result in cross-modality alignment challenges, thus leading to suboptimal results. Considering that, a novel Gradual Alignment Strategy (GAS) will be presented to address such an issue in this stage via a cluster-to-holistic alignment way.

As shown in Fig. 5, GAS will first propose a Supplementary Graph Matching (SGM) module to explore the relations among visible and infrared clusters for cluster-level alignment. Accordingly, the pseudo labels for the target domain data can be obtained by assigning those matched results to the same identities, *i.e.*, those matched visible-infrared cluster pairs are expected to belong to the same identities. Then, a Cross-Modality Consistency Constraining (CMCC) module will be further designed to reduce such noise from the misalignments in SGM and, meanwhile, mitigate the intra-domain modality discrepancies in the training process by exploring the holistic interactions among those matched visible-infrared cluster pairs.

3.3.1. Supplementary Graph Matching (SGM)

SGM aims to match the visible clusters with the infrared clusters via the following steps.

(1) Intra-modality alignment: Given the target domain data $D_t = \{D_{t,V}, D_{t,I}\}$, SGM first clusters the visible samples $D_{t,V}$ and the infrared samples $D_{t,I}$, respectively, by using CRMR proposed in the pre-training stage. Accordingly, the visible clusters $Clusters_t^V$ with $C_{t,V}$ items and infrared clusters $Clusters_t^I$ with $C_{t,I}$ items are obtained by

$$\begin{aligned} Clusters_t^V &= \text{CRMR}(D_{t,V}), \\ Clusters_t^I &= \text{CRMR}(D_{t,I}). \end{aligned} \quad (26)$$

Accordingly, their center memories $\mathbb{M}_{t,V}$ and $\mathbb{M}_{t,I}$ can also be initialized by using Eq. (6).

(2) Inter-modality alignment: Considering that the clusters $Clusters_t^V$ and $Clusters_t^I$ are unmatched, *e.g.*, the first cluster from $Clusters_t^V$ and that from $Clusters_t^I$ usually belong to different person identities, SGM employs the Hungarian matching algorithm [17] to find the optimal matching result

$$\mathbf{m} = \{\mathbf{m}(n_{t,V}, n_{t,I}) \mid n_{t,V} = 1, 2, \dots, C_{t,V}; n_{t,I} = 1, 2, \dots, C_{t,I}\} \in \mathbb{R}^{1 \times C_{t,V} C_{t,I}} \quad (27)$$

for the clusters $Clusters_t^V$ and $Clusters_t^I$. Here, $\mathbf{m}(n_{t,V}, n_{t,I})$ indicates whether the $n_{t,V}$ -th cluster within $Clusters_t^V$ and the $n_{t,I}$ -th cluster within $Clusters_t^I$ belong to the same person identity ($\mathbf{m}(n_{t,V}, n_{t,I}) = 1$) or not ($\mathbf{m}(n_{t,V}, n_{t,I}) = 0$).

Accordingly, through the optimization of the Hungarian matching algorithm, SGM can obtain an optimal result \mathbf{m} , which can find matched visible-infrared cluster pairs belonging to the same person identities at the lowest cost. Accordingly, those matched pairs will be assigned to the same pseudo labels.

(3) Intra-modality supplementary alignment: The intra-domain modality discrepancies between visible and infrared modalities of the target domain often lead to different numbers of clusters within the two modalities as discussed in [18], *i.e.*, $C_{t,V} \neq C_{t,I}$. Taking $C_{t,V} > C_{t,I}$ as an example, all the infrared clusters will find their matched visible clusters after the last inter-modality alignment step, while the rest of the visible clusters remain unlabeled. Considering that, SGM further designs an intra-modality supplementary alignment step to explore those unmatched visible clusters for supplementing inter-modality alignment. The basic idea is to re-assign such unmatched visible clusters to those matched visible clusters, since those unmatched visible clusters may be over-clustered and have higher probabilities of belonging to the same identity as their nearest visible clusters.

Specifically, we suppose that the visible clusters $Clusters_t^V$ are divided into matched clusters $Clusters_{t,M}^V$, and unmatched clusters $Clusters_{t,U}^V$ with $C_{t,V,M}$ items and $C_{t,V,U}$ items, respectively. Here, $C_{t,V,M} + C_{t,V,U} = C_{t,V}$. Their corresponding center memories $\mathbb{M}_{t,V}^M$ and $\mathbb{M}_{t,V}^U$ can also be obtained in a similar way as in Eq. (6). For those unmatched clusters, we first build the assignment cost matrix $\mathcal{K} = \{\mathbf{K}(n_{t,V,U}, n_{t,V,M}) \mid n_{t,V,U} = 1, 2, \dots, C_{t,V,U}; n_{t,V,M} = 1, 2, \dots, C_{t,V,M}\} \in \mathbb{R}^{1 \times C_{t,V,U} C_{t,V,M}}$. Here, $\mathbf{K}(n_{t,V,U}, n_{t,V,M})$

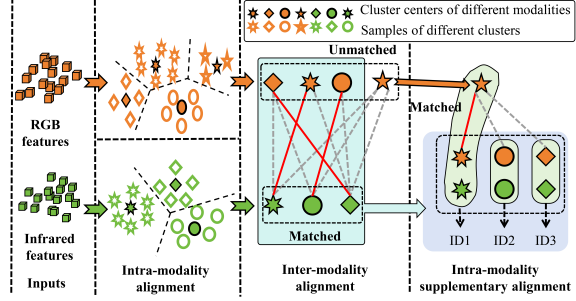


Fig. 5: Illustration of the proposed SGM module. It contains three steps: *i.e.*, Intra-modality alignment, Inter-modality alignment and Intra-modality supplementary alignment.

denotes the distance between $\mathbb{M}_{t,V}^{Um}[n_{t,V,Um}]$ and $\mathbb{M}_{t,V}^M[n_{t,V,M}]$, which is computed by

$$\begin{aligned} & \mathbf{K}(n_{t,V,Um}, n_{t,V,M}) \\ &= \beta(1 - \mathbb{M}_{t,V}^{Um}[n_{t,V,Um}]\mathbb{M}_{t,V}^M[n_{t,V,M}]^T) \\ &+ (1 - \beta)d_J(\mathbb{M}_{t,V}^{Um}[n_{t,V,Um}], \mathbb{M}_{t,V}^M). \end{aligned} \quad (28)$$

Here, $d_J(*)$ denotes the mean Jaccard distance [19] between $\mathbb{M}_{t,V}^{Um}[n_{t,V,Um}]$ and its k-reciprocal nearest neighbors in $\mathbb{M}_{t,V}^M$, which provides another distance measurement method to align the intra-domain clusters with high similarity. β is the parameter for weighting the two distances and is experimentally set to 0.2 in this paper.

Then, the corresponding nearest matched visible cluster index $n_{t,V,M}^*$ for the $n_{t,V,Um}$ -th unmatched cluster is found by optimizing

$$n_{t,V,M}^* = \arg \min_{n_{t,V,M}} \mathbf{K}(n_{t,V,Um}, n_{t,V,M}). \quad (29)$$

Finally, the label of the $n_{t,V,Um}$ -th unmatched cluster will be assigned by

$$\hat{y}_{t,V}^{Um}[n_{t,V,Um}] = \begin{cases} \hat{y}_{t,V}^M[n_{t,V,M}^*], & \text{if } \mathbf{K}(n_{t,V,Um}, n_{t,V,M}^*) < \rho, \\ -1, & \text{otherwise.} \end{cases} \quad (30)$$

Here, ρ denotes the distance threshold. It can be seen that if the distance between $\mathbb{M}_{t,V}^{Um}[n_{t,V,Um}]$ and $\mathbb{M}_{t,V}^M[n_{t,V,M}^*]$ is less than ρ , we believe that its corresponding supplementary matched clusters are reliable. Otherwise, the pseudo labels of those unmatched clusters are set to -1, which will be discarded during training. By doing so, our proposed SGM will explore the relationships among visible and infrared clusters and achieve cluster-level alignment, thus overcoming the intra-domain modality discrepancies to some extent and obtaining corresponding pseudo labels with C_t identities. Here, after filtering out those unreliable pseudo labels, $C_t \leq \min(C_{t,V}, C_{t,I})$ represents the number of person identities that simultaneously exist in both the visible and infrared modalities. Accordingly, the two memories $\mathbb{M}_{t,V}$ and $\mathbb{M}_{t,I}$ are further updated by Eq. (7) for subsequent steps, thus obtaining $\mathbb{M}_{t,V} \in \mathbb{R}^{C_t \times D}$ and $\mathbb{M}_{t,I} \in \mathbb{R}^{C_t \times D}$.

3.3.2. Cross-Modality Consistency Constraining (CMCC)

After obtaining the visible-infrared cluster pairs for the target domain data by using SGM, a Cross-Modality Consistency Constraining (CMCC) module, as shown in Fig. 6, is further designed to suppress those mismatched clusters that inevitably exist in the matching results and achieve holistic-level alignment. The basic idea is to use all the person information across visible and infrared modalities of the source and target domain data (termed holistic referring information) to assess the confidence level of each matched visible-infrared cluster pair based on the principle that a smaller distance between a pair of visible and infrared clusters indicates higher reliability.

Specifically, CMCC first constructs the holistic referring information $\mathbb{M}_{Ref} \in \mathbb{R}^{C_{Ref} \times D}$ ($C_{Ref} = C_s + C_t + C_t + C_t$) by concatenating the center memories $\mathbb{M}_{s,V}$, $\mathbb{M}_{s,I}$, $\mathbb{M}_{t,V}$ and $\mathbb{M}_{t,I}$ of the source domain data and the target domain data, *i.e.*,

$$\mathbb{M}_{Ref} = \text{Cat}(\mathbb{M}_{s,V}, \mathbb{M}_{s,I}, \mathbb{M}_{t,V}, \mathbb{M}_{t,I}). \quad (31)$$

Then, given all the visible images $x_{t,V}^{n_{id}}$ and all the infrared images $x_{t,I}^{n_{id}}$ of the n_{id} -th identity, CMCC extracts their features $\mathbf{F}_{t,V}^{n_{id}}$ and $\mathbf{F}_{t,I}^{n_{id}}$, respectively, by using the VI-ReID network, *i.e.*,

$$\mathbf{F}_{t,V}^{n_{id}} = f_{\phi}(x_{t,V}^{n_{id}}, \phi), \mathbf{F}_{t,I}^{n_{id}} = f_{\phi}(x_{t,I}^{n_{id}}, \phi). \quad (32)$$

After that, CMCC computes the similarity between those features and the holistic referring information, thus obtaining holistic similarity distributions $\mathbf{H}_{t,V}^{n_{id}}$ and $\mathbf{H}_{t,I}^{n_{id}}$ by

$$\begin{aligned} \mathbf{H}_{t,V}^{n_{id}} &= \text{Softmax}(\mathbf{F}_{t,V}^{n_{id}} \mathbb{M}_{Ref}^T), \\ \mathbf{H}_{t,I}^{n_{id}} &= \text{Softmax}(\mathbf{F}_{t,I}^{n_{id}} \mathbb{M}_{Ref}^T), \end{aligned} \quad (33)$$

where $\text{Softmax}(\ast)$ is the softmax function. Compared with directly using $\mathbf{F}_{t,V}^{n_{id}}$ and $\mathbf{F}_{t,I}^{n_{id}}$, the holistic similarity distributions $\mathbf{H}_{t,V}^{n_{id}}$ and $\mathbf{H}_{t,I}^{n_{id}}$ can exploit all the person information within the source and target domains rather than some identity-limited information within certain clusters, thus effectively assessing those generated pseudo labels. Naturally, if the visible cluster and infrared cluster are correctly matched (*i.e.*, they have the right pseudo labels), their holistic similarity distributions should be very close; otherwise, they should be far apart.

Accordingly, in the next step, CMCC assigns higher confidences/weights to those visible-infrared pairs with closer holistic similarity distributions and lower ones to those with far holistic similarity distributions. For that, CMCC computes the similarity between the holistic similarity distributions of visible-infrared pair of the n_{id} -th identity, *i.e.*, $sim_{n_{id}}$, to assess their confidence level, by

$$sim_{n_{id}} = \frac{\mathbf{H}_{t,V,center}^{n_{id}} \mathbf{H}_{t,I,center}^{n_{id}T}}{|\mathbf{H}_{t,V,center}^{n_{id}}| \times |\mathbf{H}_{t,I,center}^{n_{id}}|}. \quad (34)$$

Here, $\mathbf{H}_{t,V,center}^{n_{id}}$, and $\mathbf{H}_{t,I,center}^{n_{id}}$ are feature centers of $\mathbf{H}_{t,V}^{n_{id}}$ and $\mathbf{H}_{t,I}^{n_{id}}$, respectively, which can be obtained in a similar way by using Eq. (21). Based on such confidence value, CMCC pulls close the holistic similarity distributions $\mathbf{H}_{t,V}^{n_{id}}$ and $\mathbf{H}_{t,I}^{n_{id}}$ of the n_{id} -th identity to reduce the large intra-domain modality discrepancies by

$$\mathcal{L}_{cmcc}^{n_{id}} = sim_{n_{id}} \times \text{KL}(\log(\mathbf{H}_{t,V}^{n_{id}}/\tau), \log(\mathbf{H}_{t,I}^{n_{id}}/\tau)). \quad (35)$$

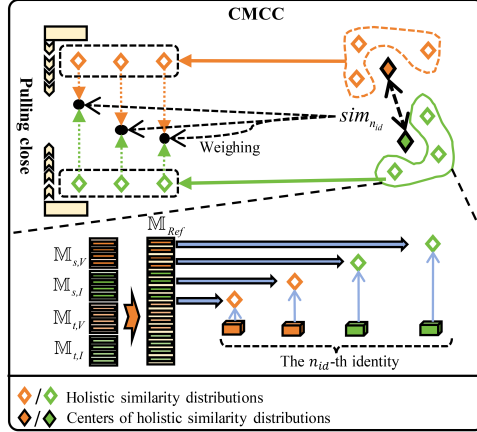


Fig. 6: Illustration of the proposed CMCC. Items in different colors represent different person identities.

Here, $KL(*)$ denotes the Kullback-Leibler Divergence function and τ is a temperature hyper-parameter. Accordingly, the \mathcal{L}_{CMCC} for all person identities in the target domain are computed by

$$\mathcal{L}_{CMCC} = \frac{1}{C_t} \sum_{n_{id}=1}^{C_t} \mathcal{L}_{cmcc}^{n_{id}}. \quad (36)$$

It can be seen that CMCC will prioritize those correctly matched samples while de-prioritizing or disregarding those incorrectly matched samples, thus simultaneously reducing the intra-domain modality discrepancies by holistic-level alignment and alleviating the disturbs from those incorrectly labeled samples during the training process. The overall loss function of our proposed DSLGA during training is

$$\mathcal{L}_{final} = \mathcal{L}_{DSAL} + \psi \mathcal{L}_{CMCC}, \quad (37)$$

where ψ is the parameter for balancing \mathcal{L}_{DSL} and \mathcal{L}_{CMCC} .

By virtue of SGM and CMCC, our proposed GAS conducts cluster-level alignment as well as holistic-level alignment to achieve reliable cross-modality alignment in the target domain. After being fine-tuned with these pseudo labels, the performance of the VI-ReID network pre-trained on the source domain data can be effectively boosted on the target domain data.

4. Experiments

4.1. Datasets and Evaluation Protocols

We conduct a new CMDA-XD testing method on top of three existing VI-ReID datasets *i.e.*, SYSU-MM01[1], RegDB[2] and LLCM[20], to train and test different UDA-VI-ReID models. As shown in Table 1, the CMDA-XD testing method consists of six modes, *i.e.*, SYSUtoLLCM, SYSUtoRegDB, LLCMtoSYSU, LLCMtoRegDB, RegDBtoSYSU and RegDBtoLLCM. Details of the proposed CMDA-XD are as follows.

4.1.1. Source domain data and target domain data of different modes

The SYSUtoLLCM mode aims to adapt the domain information from the SYSU-MM01 dataset to the LLCM dataset. For that, its training set first takes the training images and labels of the SYSU-MM01 dataset as the source domain data (including 22252 RGB images and 11909 infrared images of 395 identities) and then treats the training images of the LLCM dataset without their labels as the target domain data (including 16946 RGB images and 13975 infrared images of 713 identities). Accordingly, it takes the testing data of the LLCM dataset as its testing set (including 8680 RGB images and 7166 infrared images of 351 identities).

The SYSUtoRegDB mode, LLCMtoSYSU mode, LLCMtoRegDB mode, RegDBtoSYSU mode and RegDBtoLLCM mode are similar to SYSUtoLLCM mode, and their corresponding training and testing sets are detailed in Table 1 and Table 2.

Table 1: Source and target domain data for different modes of our proposed CMDA-XD testing method.

Evaluation modes	Source domain	Target domain	
	training set	training set	testing set
SYSUtoLLCM	SYSU-MM01 training set	LLCM training set	LLCM testing set
SYSUtoRegDB	SYSU-MM01 training set	RegDB training set	RegDB testing set
LLCMtoSYSU	LLCM training set	SYSU-MM01 training set	SYSU-MM01 testing set
LLCMtoRegDB	LLCM training set	RegDB training set	RegDB testing set
RegDBtoSYSU	RegDB training set	SYSU-MM01 training set	SYSU-MM01 testing set
RegDBtoLLCM	RegDB training set	LLCM training set	LLCM testing set

4.1.2. Evaluation modes

All experiments adhere to the established evaluation protocols commonly used in VI-ReID[1, 21]. The evaluation metrics encompass Rank-k accuracy, mean Average Precision (mAP) and the mean Inverse Negative Penalty (mINP) metric introduced in[19].

4.2. Implementation Details

The parameters of our VI-ReID network are initialized by using the pre-trained weights from the ImageNet[22] dataset. During training, each training batch consists of half source domain data and half target domain data. The batch size is set to 16×6 , *i.e.*, a total of 96 images (16 person identities with 6 samples for each identity). All images are resized to 288×144 . For different data distributions in different modes, the clustering hyperparameters in CMCR are detailed in Table 3. The parameter β in Eq. (28) is experimentally set to 0.2 to control the relative contributions of different distances for each item in \mathcal{K} . The parameter τ is set to 0.05 in Eq. (35). The parameter ψ in Eq. (37) is set to 0.5 to control the weight of L_{DSSL} and L_{CMCC} . The parameter ρ in Eq. (30) is set to 0.3 to control the threshold of supplementing clusters. We use the Adam optimizer [23] to train the model with weight decay $5e-4$. The initial learning rate is 3.5×10^{-3} and will be decayed by 10 times for every 20 epochs. The network is trained about 80 epochs. It should be noted that L_{CMCC} is just employed in the last 40 epochs.

4.3. Comparisons with State-of-the-Arts

In this subsection, we compare our proposed model with several existing SOTA VI-ReID models on the new testing method CMDA-XD. It should be noted that there

Table 2: Details of SYSU-MM01, RegDB and LLCM datasets, respectively.

Dataset	Training set				Testing set			
	RGB		Infrared		RGB		Infrared	
	number	IDs	number	IDs	number	IDs	number	IDs
SYSU-MM01	22252	395	11909	395	3803	96	301	96
RegDB	2060	206	2060	206	2060	206	2060	206
LLCM	16946	713	13975	713	484	351	7166	351

Table 3: Hyperparameters of CMCR module under different modes.

Evaluation modes	Visible modality		Infrared modality	
	ϵ_1	ϵ_2	ϵ_1	ϵ_2
SYSUtoLLCM	0.6	0.57	0.6	0.57
SYSUtoRegDB	0.33	0.3	0.33	0.3
LLCMtoSYSU	0.66	0.63	0.6	0.57
LLCMtoRegDB	0.33	0.3	0.33	0.3
RegDBtoSYSU	0.66	0.63	0.6	0.57
RegDBtoLLCM	0.6	0.57	0.6	0.57

are few existing UDA-VI-ReID methods except for our proposed model. Therefore, the other four types of ReID models, including fully-supervised VI-ReID, USL-VI-ReID, UDA-ReID and UDA-VI-ReID models are employed for comparisons. We also report the results of our proposed DSLGA under fully supervised training settings, *i.e.*, DSLGA*. It should be noted that those UDA-ReID models are designed and trained only for single-modality re-identification. Therefore, we retrain them under the proposed testing method for comparisons. The evaluation results of different methods are shown in Table 4.

4.3.1. Comparisons with Supervised Methods

As shown in Table 4, our proposed model DSLGA* achieves competitive results compared with existing SOTA models under fully supervised settings. However, a large performance margin still exists between our proposed DSLGA under UDA-VI-ReID settings and fully supervised SOTA models. Furthermore, we can also find that our proposed DSLGA under UDA-VI-ReID settings achieves competitive and even better results than those fully supervised models presented before the year 2021, *e.g.* AGW, which demonstrates the feasibility of our proposed UDA-VI-ReID method. It also indicates that the task of UDA-VI-ReID still has enormous potential in the future, appealing to a greater number of scholars who will embark on exploring the topic and contributing to the advancement of this field.

4.3.2. Comparisons with Unsupervised Methods

Experimental results in Table 4 demonstrate that our proposed DSLGA outperforms existing unsupervised methods under various settings. This proves the effectiveness of our proposed method, which can effectively transfer the learned knowledge from the source domain to the target domain.

4.3.3. Comparisons with UDA-ReID Methods

It can be seen that existing UDA-ReID methods perform poorly on our proposed testing method. This indicates that, due to the large inter-domain modality discrepancies and intra-domain modality discrepancies, existing UDA-ReID methods usually

struggle with the task of UDA-VI-ReID. Meanwhile, our proposed method achieves significant improvements over existing UDA-ReID methods. This may owe to the fact that our proposed DSLS can effectively reduce the inter-domain modality discrepancies by exploring the domain-shared information between the source and target domains, and the proposed GAS can well handle the large intra-domain modality discrepancies through a cluster-to-holistic alignment strategy.

Table 4: Performance comparisons of our proposed method and state-of-the-art methods on CMDA-XD testing method.

		LLCMtoSYSU			RegDBtoSYSU			SYSUtoLLCM			RegDBtoLLCM			SYSUtoRegDB			LLCMtoRegDB		
		All Search			All Search			InfraredtoVisible			InfraredtoVisible			VisibletoInfrared			VisibletoInfrared		
Backbone		rl	mAP	mNIP	rl	mAP	mNIP	rl	mAP	mNIP	rl	mAP	mNIP	rl	mAP	mNIP	rl	mAP	mNIP
VI-ReID	AGW 2021 [19]	47.5	47.65	35.3	-	-	-	46.4	54.8	-	-	-	-	70.05	66.37	50.19	-	-	-
	FMCNet 2022 [6]	66.34	62.51	-	-	-	-	-	-	-	-	-	-	89.12	84.43	-	-	-	-
	DEEN 2023 [24]	74.7	71.8	-	-	-	-	54.9	62.9	-	-	-	-	91.1	85.1	-	-	-	-
	WRM 2024 [25]	77.4	75.4	-	-	-	-	-	-	-	-	-	-	94.5	90.5	-	-	-	-
	CFSR-Net 2025 [26]	76.77	73.96	-	-	-	-	-	-	-	-	-	-	94.87	92.22	-	-	-	-
	DSLGA (Ours)	72.16	69.96	57.59	69.10	66.89	54.07	54.07	60.82	57.68	55.10	61.53	58.25	95.32	92.25	85.69	96.11	92.61	86.00
USL-VI-ReID	ADCA 2022 [27]	45.51	42.73	28.29	-	-	-	-	-	-	-	-	-	67.02	64.05	52.67	-	-	-
	PGM 2023 [18]	57.27	51.78	34.96	-	-	-	-	-	-	-	-	-	69.48	65.41	-	-	-	-
	DOTLA 2023 [28]	50.36	47.36	32.4	-	-	-	-	-	-	-	-	-	85.63	76.71	61.58	-	-	-
	MBCCM 2023 [29]	53.14	48.16	32.41	-	-	-	-	-	-	-	-	-	83.79	77.87	65.04	-	-	-
	BMSL 2024 [30]	57.96	53.93	-	-	-	-	-	-	-	-	-	-	70.08	66.30	-	-	-	-
	SCA-RCP 2024 [31]	51.41	48.52	33.56	-	-	-	-	-	-	-	-	-	85.59	79.12	-	-	-	-
	DMSL 2025 [32]	53.89	51.58	37.93	-	-	-	40.71	46.82	43.07	-	-	-	89.68	84.32	72.79	-	-	-
UDA-ReID	MMT 2020 [11]	7.06	9.16	7.22	6.34	8.23	6.76	6.64	8.63	7.85	7.81	10.40	9.35	5.10	6.24	6.39	6.97	7.20	6.69
	SPCL 2021 [33]	11.17	13.23	9.35	12.39	14.73	11.01	14.45	18.68	16.14	13.27	18.35	16.35	11.02	11.50	11.19	10.68	12.58	12.22
	SECRET 2022 [12]	12.30	14.92	13.03	17.42	15.04	15.72	17.54	23.35	19.22	17.10	21.86	18.66	12.62	14.18	10.85	10.39	12.28	10.21
	DMHL 2023 [34]	11.32	12.57	12.31	15.18	14.17	12.11	15.21	18.15	18.47	18.70	23.54	19.70	14.12	16.88	11.44	9.78	10.12	8.70
UDA-VI-ReID	TAA 2023 [13]	48.77	42.43	25.37	-	-	-	-	-	-	-	-	-	63.23	56.00	38.77	-	-	-
	DSLGA (Ours)	54.56	49.50	34.16	55.57	50.87	35.73	46.43	52.16	48.47	44.36	50.18	46.37	87.41	81.94	70.84	89.60	84.18	72.88

4.3.4. Comparisons with UDA-VI-ReID Methods

It can be seen that DSLGA outperforms existing UDA-VI-ReID method TAA by a large margin. This indicates that our proposed DSLS and GAS, which are specifically designed to address intra-domain and inter-domain modality discrepancies, respectively, make sense. This also demonstrates that DSLGA can effectively transfer knowledge from the source domain to the target domain.

4.4. Ablation Study

In this subsection, we validate the effectiveness of each component in our proposed DSLGA. As shown in Table 5, several variants of our proposed model are evaluated on the LLCMtoSYSU and RegDBtoSYSU modes of the CMDA-XD testing method. Here, ‘RI’ denotes the model whose parameters are randomly initialized by using Xavier [35], without pre-training and fine-tuning. ‘PRE-only’ denotes that the VI-ReID network is only trained on the source domain data and tested on the target domain data without fine-tuning. ‘DSE’, ‘DSAL’ and ‘CRMR’ denote the exploration of domain-shared information, the proposed DSAL and CRMR module in DSLS, respectively. ‘GM’ denotes that the Hungarian matching algorithm [17] is used for cross-modality matching in the fine-tuning stage. ‘SGM’ of GAS denotes employing our proposed SGM for cross-modality matching. ‘CMCC’ of GAS denotes that our proposed CMCC module is used for holistic-level alignment. It should be noted that all the compared models are trained by using the intra- and inter-modality triple loss [27] in the pre-training and fine-tuning stage, respectively, except for employing DSAL in the pre-training stage and CMCC in the fine-tuning stage. Meanwhile, all the compared models employ DBSCAN for intra-modality clustering, except for the ones using CRMR.

Table 5: Ablation study on the effectiveness of each component in DSLGA.

Index	Pre-training					Fine-tuning			Results					
	RI	Pre-Only	DSL			GM	GAS		LLCMtoSYSU			RegDBtoSYSU		
			DSE	DSAL	CRMR		SGM	CMCC	r1	mAP	mNIP	r1	mAP	mNIP
1	✓								1.28	3.03	1.69	1.28	3.03	1.69
2		✓							5.77	7.08	2.80	2.50	4.50	2.00
3			✓						35.06	35.15	21.13	35.47	35.64	22.06
4			✓	✓					37.92	36.83	24.23	36.52	36.05	23.06
5			✓	✓	✓				39.25	37.67	24.30	39.02	38.86	25.97
6			✓	✓	✓	✓			49.05	45.58	30.91	51.61	46.15	30.34
7			✓	✓	✓		✓		50.05	47.72	33.24	53.13	48.64	33.05
8			✓	✓	✓		✓	✓	54.56	49.50	34.16	55.57	50.87	35.73

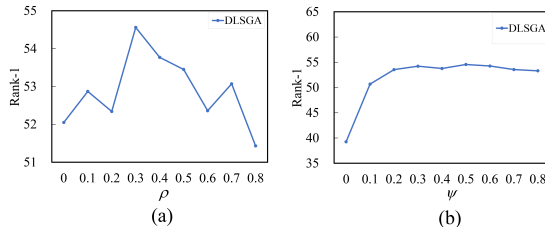


Fig. 7: Evaluation results for the hyperparameters ρ in Eq. (30) and ψ in Eq. (37).

For the pre-training stage, the results of Index 1 and Index 2 show that the VI-ReID network pre-trained on the source domain dataset is only slightly better than the randomly initialized one. This means that simply pre-training with the source domain data cannot handle the inter-domain modality discrepancies in the UDA-VI-ReID task. While the model of Index 3 achieves significant improvements over that of Index 2, which verifies the basic idea of our proposed DSLS, *i.e.*, the exploitation of domain-shared information can effectively reduce the inter-domain modality discrepancies, thus facilitating the transfer of knowledge from the source domain to the target domain. Furthermore, the model of Index 4 further boosts its performance by employing our proposed DSAL. This indicates that DSAL can further help explore more domain-shared information by pulling close the feature distributions between the source and target domain data. Besides, the results of Index 5 also show that our proposed CRMR can achieve better intra-modality clustering and generate more reliable pseudo labels than DBSCAN through its multiple clustering results refinement strategy. Eventually, our proposed DSLS effectively overcomes the inter-domain modality discrepancies, obtaining a well-initialized VI-ReID network for target domain data.

For the fine-tuning stage, compared with the results of Index 6 and Index 7, it can be seen that our proposed SGM obtains better results than the traditional GM. This means that our proposed SGM can better handle the cross-modality alignment challenges of UDA-VI-ReID than GM does by generating more reliable pseudo labels via its supplementary graph-matching based cluster-level alignment strategy. The model of Index 7, *i.e.*, our final model, achieves the best performance. This indicates that our proposed CMCC can effectively reduce the noisy information caused by mismatched pseudo labels via the holistic-level alignment strategy. Meanwhile, it also indicates that, by virtue of SGM and CMCC, GAS can effectively address the cross-modality alignment challenges caused by the large intra-domain modality discrepancies, thus

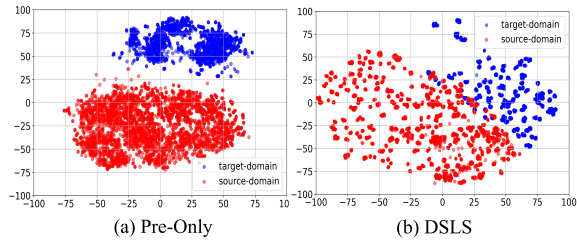


Fig. 8: Visualization of inter-domain modality discrepancies. (a) and (b) visualize the distributions of the features before and after employing the DSLS strategy, respectively.

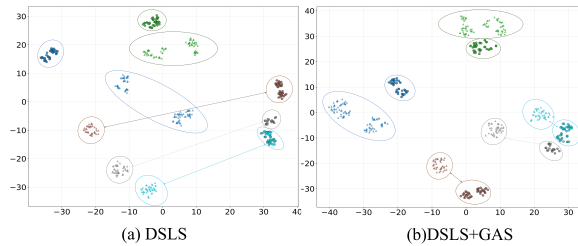


Fig. 9: Visualization of intra-domain discrepancies. (a) and (b) visualize the distributions of the features before and after employing the GAS strategy, respectively. Clusters in different colors mean different person identities. The triangular points are samples from the infrared modality, while the circular points represent samples from the visible light modality.

obtaining better fine-tuning results for the target domain data.

4.5. Parameters Analysis

4.5.1. Evaluation of ρ

The hyperparameter ρ in Eq. (30) determines the quality of the final cross-modality matching results. Thus, we evaluate its validity in this subsection on the LLCMtoSYSU dataset under all search evaluation mode. As shown in Fig. 7 (a), we vary ρ from 0 to 0.8 at intervals of 0.1. The effectiveness of ρ for Rank-1 shows an overall trend of increasing first and then decreasing with the growth of ρ . Eventually, it achieves the highest Rank-1 when $\rho = 0.3$. Accordingly, we set $\rho = 0.3$ in this paper.

4.5.2. Evaluation of ψ

The hyperparameter ψ in Eq. (37) influences the optimization process of the VI-ReID network. Thus, we evaluate its effectiveness on the LLCMtoSYSU mode under all search evaluation mode. As shown in Fig. 7 (b), we vary ψ from 0 to 0.8 at intervals of 0.1. It can be seen that the results of DSLGA for Rank-1 exhibit an overall trend of initially increasing and subsequently stabilizing. Meanwhile, it achieves the highest Rank-1 when $\psi = 0.5$. Therefore, we set $\psi = 0.5$ for our final model in this paper.

4.5.3. Visualization

As shown in Fig. 8 and Fig. 9, we visualize the inter-domain and intra-domain discrepancies of different models on the LLCMtoSYSU mode for further verifying the

effectiveness of our proposed DSLGA. All experiments are conducted on the testing dataset. As illustrated in Fig. 8, the inter-domain distance between the source and target domains under the ‘DSLGS’ strategy is smaller than that under the ‘Pre-Only’ strategy. This confirms that the domain-shared features can effectively bridge the source and target domains, thereby reducing the inter-domain modality discrepancies. Meanwhile, as depicted in Fig. 9, the feature distances between clusters sharing the same identity but originating from different modalities are reduced after applying our proposed ‘GAS’ strategy. The results indicate that our cluster-to-holistic alignment approach successfully: (1) produces accurate cross-modality pseudo-labels, and (2) filters out mismatched correspondences, consequently reducing intra-domain modality discrepancies.

5. Conclusion

This paper presents a novel two-stage model, *i.e.*, Domain-Shared Learning and Gradual Alignment (DSLGA) model, for UDA-VI-ReID, which effectively transfers the knowledge learned from the source domain data to the target domain data without annotating the latter. By virtue of its domain-shared information exploration-based Domain-Shared Learning Strategy (DSLGS), DSLGA overcomes the large inter-domain modality discrepancies and pre-trains a well-initialized VI-ReID network for the target domain data by using those labeled source domain data. Owing to the proposed Gradual Alignment Strategy (GAS), DSLGA gradually addresses the cross-modality alignment challenges caused by the intra-domain modality discrepancies in a cluster-to-holistic alignment way, *i.e.*, first generating reliable pseudo-labels in the cluster level by the Supplementary Graph Matching (SGM) module and then suppressing those incorrect pseudo labels in the holistic level by the Cross-Modality Consistency Constraining (CMCC) module. Finally, a new testing method *i.e.*, CMDA-XD, is constructed for training and testing different UDA-VI-ReID models. Extensive experiments demonstrate that our method significantly outperforms existing domain adaptation methods for ReID and even some supervised methods under various settings, pushing UDA-VI-ReID to real-world deployment.

6. Acknowledgments

This work is supported by the National Natural Science Foundation of China under Grant No.61803290 and No.61773301, and by the Fundamental Research Funds for the Central Universities under Grant No.ZYTS24022.

References

- [1] A. Wu, W.-S. Zheng, H.-X. Yu, S. Gong, J. Lai, Rgb-infrared cross-modality person re-identification, in: Proc. IEEE/CVF Int. Conf. Comput. Vis., 2017, pp. 5390–5399.

- [2] D. T. Nguyen, H. G. Hong, K. W. Kim, K. R. Park, Person recognition system based on a combination of body images from visible light and thermal cameras, *Sensors* 17 (3) (2017).
- [3] K. Zheng, C. Lan, W. Zeng, Z. Zhang, Z.-J. Zha, Exploiting sample uncertainty for domain adaptive person re-identification, in: *Proc. AAAI Conf. Artif. Intell.*, Vol. 35, 2021, pp. 3538–3546.
- [4] J. Li, S. Zhang, Joint visual and temporal consistency for unsupervised domain adaptive person re-identification, in: *Proc. Eur. Conf. Comput. Vis.*, 2020, p. 483–499.
- [5] Y. Tian, X. Peng, L. Zhao, S. Zhang, D. N. Metaxas, Cr-gan: learning complete representations for multi-view generation, *arXiv: 1806.11191* (2018).
- [6] Q. Zhang, C. Lai, J. Liu, N. Huang, J. Han, Fmcnet: Feature-level modality compensation for visible-infrared person re-identification, in: *Proc. IEEE/CVF Conf. Comput. Vis. Pattern Recognit.*, 2022, pp. 7349–7358.
- [7] M. Ye, W. Ruan, B. Du, M. Z. Shou, Channel augmented joint learning for visible-infrared recognition, in: *Proc. IEEE/CVF Conf. Comput. Vis. Pattern Recognit.*, 2021, pp. 13567–13576.
- [8] M. Ye, Z. Wang, X. Lan, P. C. Yuen, Visible thermal person re-identification via dual-constrained top-ranking., in: *Proc. Int. Joint Conf. Artif. Intell.*, Vol. 1, 2018, p. 2.
- [9] H. Liu, S. Ma, D. Xia, S. Li, Sfanet: A spectrum-aware feature augmentation network for visible-infrared person reidentification, *IEEE Trans. Neural Netw. Learn. Syst.* 34 (4) (2021) 1958–1971.
- [10] Y. Huang, Q. Wu, J. Xu, Y. Zhong, Z. Zhang, Unsupervised domain adaptation with background shift mitigating for person re-identification, *Int. J. Comput. Vis.* (2021) 2244–2263.
- [11] Y. Ge, D. Chen, H. Li, Mutual mean-teaching: Pseudo label refinery for unsupervised domain adaptation on person re-identification, *arXiv: 2001.01526* (2020).
- [12] T. He, L. Shen, Y. Guo, G. Ding, Z. Guo, Secret: Self-consistent pseudo label refinement for unsupervised domain adaptive person re-identification, in: *Proc. AAAI Conf. Artif. Intell.*, 2022, p. 879–887.
- [13] B. Yang, J. Chen, X. Ma, M. Ye, Translation, association and augmentation: Learning cross-modality re-identification from single-modality annotation, *IEEE Trans. Image Process.* 32 (2023) 5099–5113.
- [14] J. Liu, Y. Sun, F. Zhu, H. Pei, Y. Yang, W. Li, Learning memory-augmented unidirectional metrics for cross-modality person re-identification, in: *Proc. IEEE/CVF Conf. Comput. Vis. Pattern Recognit.*, 2022, pp. 19366–19375.

- [15] I. Goodfellow, J. Pouget-Abadie, M. Mirza, B. Xu, D. Warde-Farley, S. Ozair, A. Courville, Y. Bengio, Generative adversarial nets, in: Proc. 31st Int. Conf. Neural Inf. Process. Syst., Vol. 27, 2014.
- [16] M. Ester, H.-P. Kriegel, J. Sander, X. Xu, et al., A density-based algorithm for discovering clusters in large spatial databases with noise, *Knowledge Discovery and Data Mining* 96 (34) (1996) 226–231.
- [17] D. Bruff, The assignment problem and the hungarian method, *Notes for Math* 20 (29-47) (2005) 5.
- [18] Z. Wu, M. Ye, Unsupervised visible-infrared person re-identification via progressive graph matching and alternate learning, in: Proc. IEEE/CVF Conf. Comput. Vis. Pattern Recognit., 2023, pp. 9548–9558.
- [19] M. Ye, J. Shen, G. Lin, T. Xiang, L. Shao, S. C. H. Hoi, Deep learning for person re-identification: A survey and outlook, *IEEE Trans. Pattern Anal. Mach. Intell.* 44 (6) (2022) 2872–2893.
- [20] Y. Zhang, H. Wang, Diverse embedding expansion network and low-light cross-modality benchmark for visible-infrared person re-identification, in: Proc. IEEE/CVF Conf. Comput. Vis. Pattern Recognit., 2023, pp. 2153–2162.
- [21] M. Ye, X. Lan, J. Li, P. Yuen, Hierarchical discriminative learning for visible thermal person re-identification, in: Proc. AAAI Conf. Artif. Intell., Vol. 32, 2022.
- [22] J. Deng, W. Dong, R. Socher, L.-J. Li, K. Li, L. Fei-Fei, Imagenet: A large-scale hierarchical image database, in: Proc. IEEE/CVF Conf. Comput. Vis. Pattern Recognit., Ieee, 2009, pp. 248–255.
- [23] D. Kinga, J. B. Adam, et al., A method for stochastic optimization, in: International conference on learning representations (ICLR), Vol. 5, San Diego, California;, 2015, p. 6.
- [24] Y. Zhang, H. Wang, Diverse embedding expansion network and low-light cross-modality benchmark for visible-infrared person re-identification, in: Proc. IEEE/CVF Conf. Comput. Vis. Pattern Recognit., 2023, pp. 2153–2162.
- [25] Y. Wu, L.-C. Meng, Y. Zichao, S. Chan, H.-Q. Wang, Wrim-net: Wide-ranging information mining network for visible-infrared person re-identification, in: Proc. Eur. Conf. Comput. Vis., Springer, 2024, pp. 55–72.
- [26] X. Chen, Y. Yan, J.-H. Xue, N. Wang, H. Wang, Consistency-driven feature scoring and regularization network for visible–infrared person re-identification, *Pattern Recognition* 159 (2025) 111131.
- [27] B. Yang, M. Ye, J. Chen, Z. Wu, Augmented dual-contrastive aggregation learning for unsupervised visible-infrared person re-identification, in: Proc. ACM Int. Conf. Multimedia, 2022, p. 2843–2851.

- [28] D. Cheng, X. Huang, N. Wang, L. He, Z. Li, X. Gao, Unsupervised visible-infrared person reid by collaborative learning with neighbor-guided label refinement, in: Proc. ACM Int. Conf. Multimedia, 2023, pp. 7085–7093.
- [29] D. Cheng, L. He, N. Wang, S. Zhang, Z. Wang, X. Gao, Efficient bilateral cross-modality cluster matching for unsupervised visible-infrared person reid, in: Proc. ACM Int. Conf. Multimedia, 2023, pp. 1325–1333.
- [30] Z. Pang, L. Zhao, Y. Liu, G. Sharma, C. Wang, Inter-modality similarity learning for unsupervised multi-modality person re-identification, IEEE Trans. Circuits Syst. Video Technol. 34 (10) (2024) 10411–10423.
- [31] Z. Li, H. Liu, X. Peng, W. Jiang, Inter-intra modality knowledge learning and clustering noise alleviation for unsupervised visible-infrared person re-identification, IEEE Trans. TKDE 36 (8) (2024) 3934–3947.
- [32] L. Dai, Z. Luo, Y. Ling, J. Chai, S. Li, Dual-modality-shared learning and label refinement for unsupervised visible-infrared person reid, ACM Trans. Multimedia Comput. Commun. Appl. (2025) 1551–6857.
- [33] Y. Ge, F. Zhu, D. Chen, R. Zhao, et al., Self-paced contrastive learning with hybrid memory for domain adaptive object re-id, in: Proc. 31st Int. Conf. Neural Inf. Process. Syst., Vol. 33, 2020, pp. 11309–11321.
- [34] F. Chen, N. Wang, J. Tang, P. Yan, J. Yu, Unsupervised person re-identification via multi-domain joint learning, Pattern Recognition 138 (2023) 109369.
- [35] X. Glorot, Y. Bengio, Understanding the difficulty of training deep feedforward neural networks, in: Proc. 13th Int. Conf. Artif. Intell., 2010, pp. 249–256.